Nano Energy 76 (2020) 105068

Contents lists available at ScienceDirect

Nano Energy

journal homepage: http://www.elsevier.com/locate/nanoen

Stabilizing lithium metal anode by molecular beam epitaxy grown uniform and ultrathin bismuth film

Tao Chen [a], Fanbo Meng [b], Zewen Zhang [a], Junchuan Liang [a], Yi Hu [a], Weihua Kong [a], Xiao Li Zhang [c], Zhong Jin [a,*]

[a] Key Laboratory of Mesoscopic Chemistry of MOE, Jiangsu Key Laboratory of Advanced Organic Materials, School of Chemistry and Chemical Engineering, Shenzhen Research Institute of Nanjing University, Nanjing University, Nanjing, 210023, China
[b] School of Mechanical and Electrical Engineering, Xidian University, Xi'an, 710000, China
[c] School of Materials Science and Engineering, Zhengzhou University, Zhengzhou, 450001, China

ARTICLE INFO

Keywords:
Molecular beam epitaxy
Lithium metal anodes
Ultrathin bismuth film
Lithium-bismuthide alloy
Lithiophilic nucleation site

ABSTRACT

Lithium metal anode is regarded as an attractive option for next-generation high-energy-density rechargeable batteries. However, the unstable solid-electrolyte interphases between lithium anode and electrolyte lead to uncontrolled growth of lithium dendrites. Herein, we describe the surface reconstruction of Li anode by molecular beam epitaxy deposition of an ultrathin and compact bismuth film. During Li plating process, the electrochemical active bismuth film is prone to form a close-knit lithiophilic lithium-bismuthide (Li_xBi) alloy layer through electrochemical alloying with lithium metal. Benefiting from its high ionic conductivity, lithiophilic characteristics, high chemical stability, good mechanical properties and air/moisture tolerance, the Li_xBi-rich layer efficiently inhibit the parasitic reactions between Li anode and electrolyte, and thus favor a dendrite-free Li plating/stripping process, as verified by electrochemical tests and in-depth analyses. Symmetric cells with Bi-coated Li electrodes show a stable and dendrite-free cycling behavior at 1.0 mAh cm^{-2} for 300 h and superior rate performance up to 5.0 mA cm^{-2}. When Bi-coated lithium anodes are paired with a $LiNi_{0.5}Co_{0.2}Mn_{0.3}O_2$ cathode, a stable cycling life for over 300 cycles at 0.5C with a high capacity retention rate of 97% is obtained. This work provides new insights and strategies for the construction of Li-rich alloy layers on lithium metal surface via molecular beam epitaxy that enables dendrite-free and high-performance lithium metal batteries.

1. Introduction

Rechargeable lithium-ion batteries (LIBs) based on intercalation chemistries are approaching their energy-density ceiling due to the inherent limited capacity (372 mAh g^{-1} for graphite anode), which cannot fully satisfy the ever-increasing demands for electric vehicle and smart grid storage [1]. As a lightweight anode material, metallic lithium has currently regained tremendous attention, owing to its high theoretical specific capacity (3860 mAh g^{-1}) and low reduction potential (3.04 V vs. standard hydrogen electrode, SHE) [2–5]. Despite many advantages, the batteries based on metallic Li anodes are still plagued with three severe issues that hinder their practical applications. (1) Metallic lithium anode is susceptible to undesired/uncontrolled growth of lithium dendrites, due to the uneven distribution of Li ions on the electrode surface during Li plating [6,7]. The accumulated dendritic Li could penetrate separators between electrodes, eventually causing short-circuit of batteries and serious safety issue [8,9]. (2) Li dendrites are easy to fall off from the current collectors during Li stripping process, which causes the formation of "dead Li" and the depletion of fresh Li. In addition, the formation of dead Li at the edge of an electrode exposed to pressure-free space also causes the increased Li consumption during cycling [10]. (3) Lithium anode are easy to react with nonaqueous electrolytes and form an unstable solid electrolyte interphase (SEI) on the surface [11]. The rupture and reconstructions of SEI are difficult to avoid during the repeated plating/stripping process, leading to the exhaustion of limited Li and lean electrolyte in practical Li metal batteries [12].

To circumvent the above issues regarding lithium metal anode, several strategies have been proposed to suppress dendritic Li growth and stabilize Li metal anode, including: (1) optimizing the SEI compositions by adding electrolyte additives to reinforce the SEI film [13,14]; (2) utilizing high-modulus solid-state electrolytes to block dendrite

* Corresponding author.
E-mail address: zhongjin@nju.edu.cn (Z. Jin).

https://doi.org/10.1016/j.nanoen.2020.105068
Received 18 May 2020; Received in revised form 31 May 2020; Accepted 4 June 2020
Available online 4 July 2020

growth [15–17]; (3) modifying the separator with functional compositions or surface groups to homogenize Li-ion flux and achieve uniform Li electrodeposition [18–20]; (4) precoating the Li surface with artificial protective layers to prevent direct contact between Li metal and electrolytes [21–26]; Although these strategies have boosted the performances of Li anode to a certain extent, further efforts/optimizations are still required to enable long cycle life and dendrite-free lithium deposition towards safe and high-energy lithium metal batteries. For instance, owing to the gradual loss of electrolyte additives, the SEI film on lithium surface formed by the introduction of electrolyte additives is not capable of continuously suppressing lithium dendrite growth during long-term cycling [27–29]. On the other hand, the utilization of solid-state electrolyte is hindered by their fragility feature and high interfacial resistance with electrodes [30,31]. Besides, the issues of

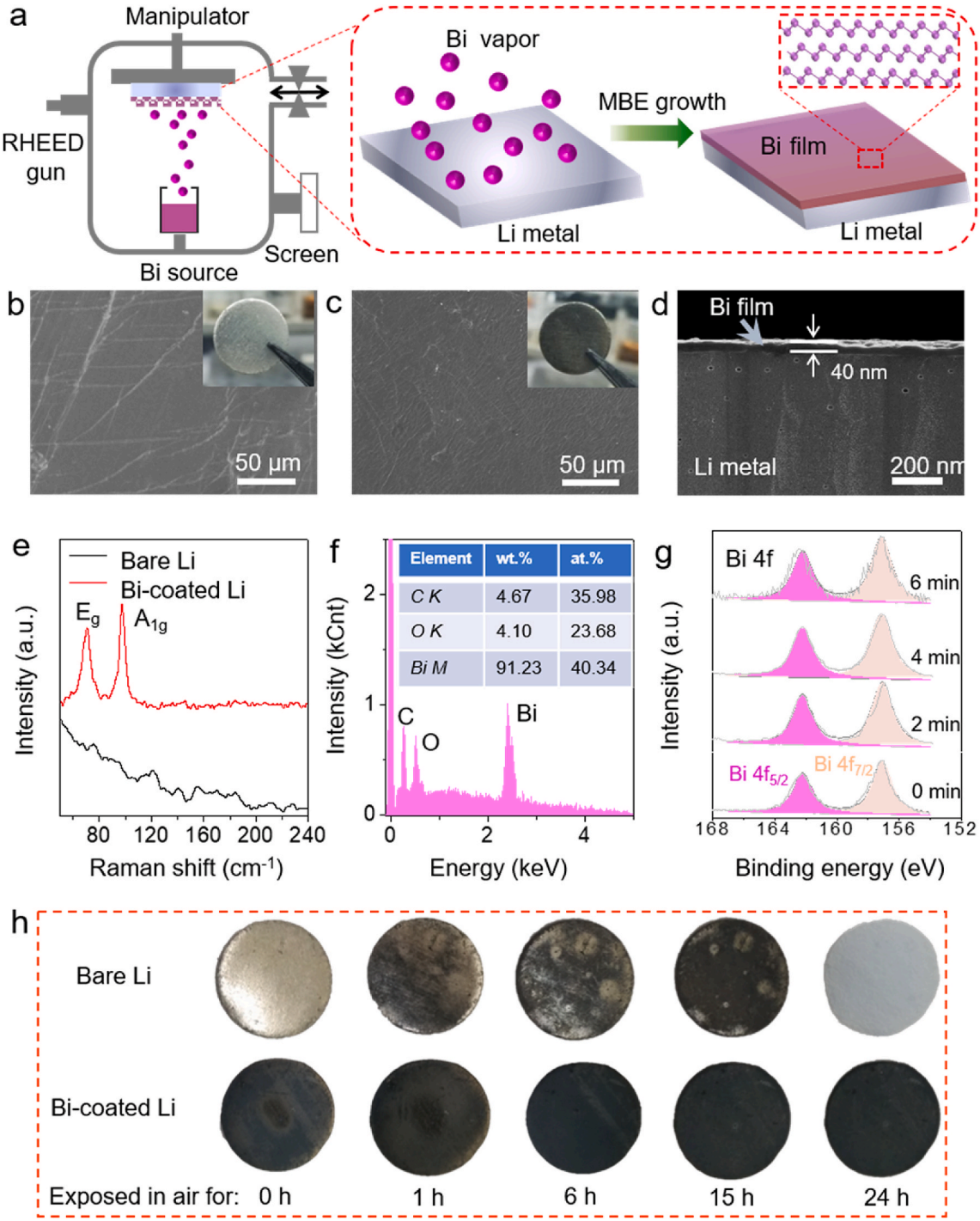

Fig. 1. Fabrication and characterization of Bi-coated Li foils. (a) Schematic diagrams of the growth of uniform and thin Bi film on lithium substrate by evaporating Bi metal precursor in the ultrahigh-vacuum MBE apparatus. (b, c) Top-view SEM images of (b) bare Li and (c) Bi-coated Li foils. The insets in (b, c) are the optical images of bare Li and (c) Bi-coated Li foils, respectively. (d) Cross-sectional SEM image of Bi-coated Li foils cut by focused ion beam (FIB) sectioning. (e) Raman spectra of bare Li and Bi-coated Li foils. (f) EDX spectra of Bi-coated Li foil surface. (g) In-depth XPS profile analysis at Bi 4f region of the Bi-coated Li foil surface after Ar-ion sputtering bombardment for different periods. (h) Optical photographs of bare Li and Bi-coated Li foils after exposed in air with relative humidity of 30–35% for different durations.

separator modification associated with poor mechanical strength and sacrificed ionic conductivity still remain unsolved [32]. Compared to the other three strategies, the utilization of an artificial protective layer is a promising choice to continuously suppress dendrite growth and overcome the surface inhomogeneity and mechanical instability of electrolyte-derived SEI film, ensuring long-term stable Li stripping/-plating. Nevertheless, artificial protective layer usually undergoes the compositional evolution and large volume variation during cycling, which may result in the degradation of protective effect. Therefore, it is challenging to construct a chemically stable and compositionally homogeneous interfacial layer that can effectively regulate homogeneous deposition of Li and meanwhile reduce parasitic side reactions during long-term cycling.

Thin film deposition technologies have been proposed to stabilize the surface of Li metal, including magnetron sputtering [33], atomic layer deposition (ALD) [34] and molecular layer deposition (MLD) [35]. Promoted by controlling the thickness and compositions of protective layer at atomic level, the cycling performance and rate capability of Li metal batteries can be greatly enhanced. As a precisely-controllable thin film deposition technology, molecular beam epitaxy (MBE) has prominent advantages for large-scale growth of atomic-scale-uniform film by accurately controlling the molecular beam flux, the growth temperature and the rotation/tilting of sample stage [36]. Herein, we report the deposition of a ultrathin and uniform bismuth film on Li metal surface through MBE technology by thermally evaporating Bi precursor under ultrahigh vacuum. The electrochemically active bismuth film is prone to form a chemically stable Li_xBi alloy phase layer by in situ alloying with lithium, thus can minimize the detrimental side reaction between Li and electrolyte. Moreover, the ionic conductive Li_xBi alloy layer offers lithiophilic nucleation sites to guide homogeneous lithium plating, and meanwhile facilitates rapid ion transport through the electrode-electrolyte interface, realizing dendrite-free lithium deposition. Furthermore, the Bi-coated Li anode shows excellent humid resistance even when exposed to air atmosphere with the relative humidity (RH) of 30–35%. As a result, the Bi-coated Li anode exhibits superior cycling stability for over 300 h at 1.0 mA cm^{-2} and rate performance up to 5 mA cm^{-2} in symmetric cells. A full cell paired Bi-coated Li anode with $LiNi_{0.5}Co_{0.2}Mn_{0.3}O_2$ cathode can deliver a stable operation life for over 200 cycles.

2. Results and discussion

As schematically illustrated in Fig. 1a, uniform and ultrathin bismuth film was directly grown on the surface of lithium foil using an ultrahigh-vacuum MBE apparatus equipped with a reflection high-energy electron diffraction (RHEED) gun. The bismuth film was deposited by evaporating high-purity Bi metal source from a large-orifice pocket electron-beam evaporator. To achieve the MBE growth of homogeneous bismuth film, ultrahigh vacuum with basic pressure of lower than 2×10^{-10} Torr is very necessary [37].

As shown in Fig. 1b, scanning electron microscopy (SEM) image of bare Li foil shows a smooth and flat surface. From the top-view SEM images of Bi-coated Li foil, it is evident that the entire surface of the lithium metal was compactly covered with uniform bismuth film without cracks and holes, benefited from the homogeneous MBE growth. For comparison, the optical images of bare Li and Bi-coated Li electrode (the insets of Fig. 1b and c) revealed that the silvery lithium foil turns into gray color after the coating of bismuth film. Cross-sectional SEM image of Bi film was obtained using focused ion beam (FIB) sectioning. As shown in Fig. 1d, by taking 2 h of MBE growth, continuous Bi film with an optimal ultrathin thickness of around 40 nm was deposited and firmly adhered to the underlying lithium substrate. The thickness of MBE-grown Bi film can be conveniently adjusted by the deposition time. By increasing the deposition time to 4 h, the thickness of Bi film on Li surface is increased to approximately 100 nm (Fig. S1), while numerous randomly-distributed Bi nanoparticles were also formed the surface of Bi film, as shown in Fig. S2. Considering that the surface roughness and inhomogeneity may cause uneven Li electrodeposition, the Bi-coated Li electrodes with the deposition time of 2 h were chosen for further studies.

The compositions and chemical states of Bi-coated Li foil were further verified by Raman spectroscopy and energy dispersive X-ray spectroscopy (EDX) analysis. The Raman spectrum of the Bi-coated Li surface shows two characteristic peaks at 70.9 cm^{-1} and 97.8 cm^{-1} (Fig. 1e), corresponding to the E_g and A_{1g} stretching modes of Bi–Bi bonds, respectively [38,39]. Moreover, there is no Raman peak of oxidation phases or impurity detected from the Bi-coated Li electrodes. The corresponding Raman mapping on the intensity of A_{1g} mode confirms the homogeneous distribution of Bi component in the surficial layer (Fig. S3). EDX spectrum clearly show that bismuth is the major element in the film (Fig. 1f). The compositions of Bi-coated Li metal surface were further probed by in-depth X-ray photoelectron spectroscopy (XPS) profile analysis. The surface of Bi-coated Li metal was peeled by different thicknesses via the bombardment of Ar-ion sputtering, for accurate in-depth XPS profiling. As the time of Ar-ion sputtering increased, the Bi 4f XPS spectra clearly show the characteristic peaks of zero-valent Bi metal as the dominated peaks without the sign of impurities, indicating the uniformly distributed and single-component Bi film deposition on Li metal surface (Fig. 1g).

To intuitively elucidate the air stability and humidity tolerance performance of MBE-grown Bi film, the bare Li and Bi-coated Li foils were exposed to air atmosphere with RH of 30–35% for comparison. After exposure to air for 1 h, the silvery color of bare Li foil gradually turned to grayish black and the surface became roughened (Fig. 1h). For Bi-coated Li electrode, no visible change in color and surface roughness was observed even after exposed to air for 24 h, indicating that the MBE-grown Bi film as a physical barrier can effectively protect the underneath Li metal from the oxidation in ambient air.

To illustrate the electrochemical stability of Bi-coated Li electrodes, time-dependent electrochemical impendence spectra (EIS) of Li|Li symmetric cells with bare Li or Bi-coated Li electrodes were measured (Fig. S4). All cells were tested using the electrolyte of 1 M $LiPF_6$ in ethylene carbonate/dimethyl carbonate (EC/DMC, 1:1 v/v). According to the analysis in Figs. S4c and d, the interfacial charge transfer resistance (R_{ct}) of symmetric cells with bare Li electrodes increased from 238 to 498.8 Ω after resting for 96 h, indicating that the side reactions between bare Li electrodes and electrolyte have occurred. In contrast, the symmetric cell with Bi-coated Li electrodes possesses a lower interfacial resistance of 75.5 Ω after 0.5 h, which increases slightly to 93.4 Ω after 96 h. This result suggests that the MBE-deposited Bi film can facilitate the interfacial transport of Li ions, and is also capable of protecting Li metal from the side reactions with electrolyte.

To evaluate the electrochemical performances of Bi-coated Li electrode, the Li plating/stripping behavior of symmetrical cells during continuous long-term cycling were investigated. Fig. 2a–c compares the time-resolved voltage profiles of the cells with bare Li or Bi-coated Li electrodes during cycling at different current densities. Remarkably, the symmetric cells with Bi-coated Li electrodes exhibited stable Li plating/stripping behavior and low overpotentials for over 300 h at the current density of 1 mA cm^{-2} and for 150 h at the current density of 2 mA cm^{-2}, respectively. In sharp contrast, the symmetric cells with bare Li electrodes showed poor cycling stability (only 150 h at 1 mA cm^{-2} and 55 h at 2 mA cm^{-2}). When the current density further increased to 4 mA cm^{-2}, the cells with Bi-coated Li electrodes still maintained stable voltage profile for 120 h. However, the cells with bare Li electrodes exhibited significant voltage fluctuation starting from 27 h, which can be attributed to the continuous depletion of electrolyte and internal microscale short-circuit caused by Li dendrite penetration. The voltage hysteresis is equal to a sum of the overpotentials of Li stripping and plating, which is closely related to current density, charge transfer resistance, and interfacial stability. Therefore, the distinct differences in voltage hysteresis/polarization are further emphasized by the magnified

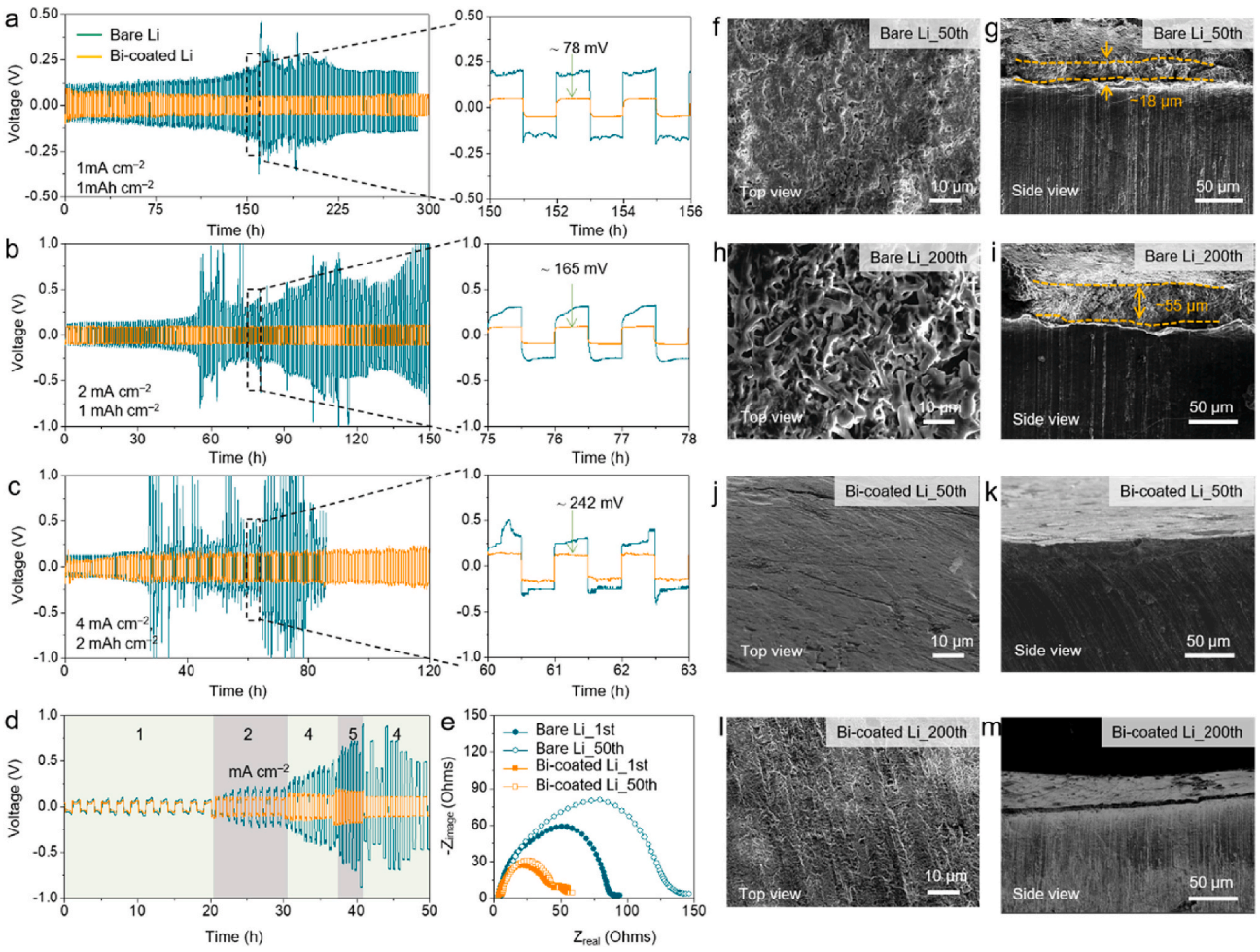

Fig. 2. Electrochemical performance of symmetric cells with Bi-coated Li electrodes and SEM investigation of Bi-coated Li electrodes. (a–c) Voltage profiles of symmetric cells with bare Li and Bi-coated Li electrodes at (a) 1 mA cm^{-2} with a capacity of 1 mAh cm^{-2}, (b) 2 mA cm^{-2} with a capacity of 1 mAh cm^{-2}, and (c) 4 mA cm^{-2} with a capacity of 2 mAh cm^{-2}. The magnified voltage profiles of given cycles were shown at the right side. (d) Rate performances of symmetric cells with bare Li and Bi-coated Li electrodes at various current densities from 1 to 5 mA cm^{-2}. (e) EIS spectra of the symmetric cells with bare Li and Bi-coated Li electrodes after the 1st and 50th cycle at 4 mA cm^{-2}. (f, h) Top-view and (g, i) cross-section SEM images of bare Li electrodes after the 50th and 200th cycles at a current density of 1 mA cm^{-2}, respectively. (j, k) Top-view and (l, m) cross-section SEM images of Bi-coated Li electrodes after the 50th and 200th cycles at a current density of 1 mA cm^{-2}, respectively.

voltage profiles of the symmetric cells with bare Li and Bi-coated Li electrodes. For the Bi-coated Li electrode, the voltage hysteresis steadily maintained at around 78, 165 and 242 mV at the current densities of 1, 2 and 4 mA cm^{-2}, respectively. However, the voltage hysteresis of the cells with bare Li electrodes gradually increased to 380 mV after testing for 150 h at 1 mA cm^{-2}, accompanied by random voltage oscillations/fluctuations. At elevated current densities of 2 and 4 mA cm^{-2}, sudden voltage fluctuations/failures of the symmetric cells with bare Li electrodes occurred after only 55 and 27 h, respectively. These results suggested that the uniform Bi film deposited on Li metal surface is very helpful for improving the stability of continuous Li plating/stripping. The cross-sectional view of Bi-coated Li electrode plated with 2 mAh cm^{-2} (10–12 μm thick) of lithium shows smooth surface after lithium deposition (Fig. S5).

The rate performances of bare Li and Bi-coated Li electrodes at various current densities are also compared and illustrated in Fig. 2d. As expected, the symmetric cell with Bi-coated Li electrodes shows a stable voltage plateau with a low overpotential even at 5 mA cm^{-2}, whereas the cell with bare Li electrodes exhibits significant increase in voltage hysteresis under the same current densities. The excellent rate performance of Bi-coated Li electrodes also demonstrates the outstanding compatibility and robustness of MBE-grown Bi film for Li plating/stripping. EIS analysis was conducted to further analyze the interfacial resistance and stability at the electrode/electrolyte interfaces. After one cycle, the interfacial resistance of the cell with bare Li electrodes is 89 Ω (Fig. 2e), which is almost twice high that of the cells with Bi-coated Li electrodes (45 Ω). Moreover, the cell with Bi-coated Li electrodes maintained almost unchanged interfacial resistance and charge transfer impedance after 50 cycles, while the resistance of the cell with bare Li electrodes markedly increased. It can be explained by the favorable ion transport characteristics and cycling stability of the MBE-grown Bi film during Li stripping and plating process.

The structural stability of Li anode/electrolyte interface is another critical factor for the cycling life of lithium metal batteries. To gain insight into the Li-plating behavior of MBE-grown Bi film, the morphology evolution of bare Li and Bi-coated Li electrodes after cycling was characterized by SEM observation (Fig. 2f-m). The electrodes were retrieved from the symmetric cells after cycling, followed by carefully rinsed with dimethyl carbonate. The top-view and cross-section SEM images of bare Li and Bi-coated Li electrodes were collected after 50 and 200 cycles at 1.0 mA cm^{-2} with a fixed capacity of 1 mAh cm^{-2}. As shown in Fig. 2f, the cycled bare Li foil exhibits uneven and rough surface after 50 cycles, which is thoroughly covered by mossy Li dendrites. From the cross-section SEM image (Fig. 2g), it is seen that the

cycled Li electrode shows porous dendritic Li layer with a thickness of ~18 μm. More seriously, after 200 cycles, the bare Li electrode displays a much rougher surface (Fig. 2h) and the thickness of porous dendritic layer has increased to ~55 μm (Fig. 2i). This phenomenon indicates that the unstable SEI layer formed on the surface of bare Li electrode could not effectively protect fresh Li against the corrosion of electrolyte and the growth of Li dendrites. As expected, a relatively flat and smooth surface can be maintained for Bi-coated Li electrodes even after 200 cycles, indicating a dendrite-free Li deposition morphology (Fig. 2j-m). The dendrite-free Li electrodeposition behavior of Bi-coated Li electrodes indicates that the MBE-grown ultrathin Bi film can effectively suppress Li dendrite growth and achieve stable Li plating/stripping.

XPS characterization was conducted to identify the chemical composition evolution of the SEI formed on Bi-coated Li electrodes after Li plating of the 1st and 50th cycle. After the 1st plating process, the Bi 4f spectrum shows major characteristic peaks of Bi-coated Li electrode at 156.6 and 161.7 eV, indicating the lithiation of Bi layer to form Li_xBi alloy upon plating (Fig. 3a) [40]. In the Li 1s spectrum, three peaks located at 54.5, 55.4, and 56.3 eV are assigned to Li_2CO_3, Li_xBi, and LiF, respectively. The O 1s spectrum shows three peaks at 530.2, 532.1 and 533.4 eV, corresponding to C═O, Li_2CO_3 and C–O species, respectively. The characteristic peaks in C 1s spectrum confirm the presence of Li_2CO_3, C═O, C–O and C–C species after the 1st cycle. In combination with Bi 4f, Li 1s, O 1s and C 1s spectra (Fig. 3b), it can be concluded that the major species in the Li_xBi-rich surface layer after 50th cycle plating are Li_xBi, LiF and Li_2CO_3. In the Li 1s spectrum, the increment of tough LiF in SEI layer is attributed to the decomposition of $LiPF_6$ salt. The inorganic components of Li_2CO_3 and LiF in Li_xBi-rich layer is helpful to suppress dendrite growth and guide uniform Li electrodeposition [41, 42]. Besides, the main compositions of the Li_xBi-rich layer are essentially unchanged after long-term cycling. It revealed the Li_xBi-rich interfacial layer plays a key role in guiding homogeneous Li plating/stripping, facilitating rapid ion diffusion and preventing the detrimental reaction between Li and electrolyte during long-term cycling.

We also characterized the side-view morphology of Bi-coated Li electrode at different cycling stages to further investigate its lithiation/delithiation behavior. As shown in Fig. S6, the plated Li is uniformly distributed on the Bi-coated Li anode without any lithium dendrites when the plating capacity reaches to 0.5 and 1.0 mAh cm^{-2}. The cross-sectional SEM image shows that the surface of Li_xBi alloy layer after Li stripped with a capacity of 1 mAh cm^{-2} still remains uncracked and intact (Fig. S6c). The electronic conductivity of Li metal electrode coated by Li_xBi-rich layer was tested via direct-current-voltage measurement. Fig. S7 shows the voltage responses of bare Li and Li_xBi-coated Li (Li_xBi/Li) electrodes by applying a constant current of 5 mA. The electronic resistivity of the Li_xBi-rich layer is measured to be $(1.1 \pm 0.12) \times 10^6$ Ω cm. Thus, the electronic conductivity (σ_e) of the Li_xBi-rich layer can be calculated to be $0.93 \pm 0.11 \times 10^{-6}$ S cm^{-1}.

To investigate the effect of MBE-grown Bi layer on suppressing dendrite growth, the morphological evolutions of bare Li and Bi-coated Li electrodes were monitored in a sealed electrochemical cell with transparent quartz window by *Operando* optical microscopy. The real-time morphology variation of the electrodes during lithium electrodeposition at a current density of 3 mA cm^{-2} was clearly visualized, as depicted in Fig. 4a and b. In the initial state, both bare Li and Bi-coated Li electrodes display a clean and smooth surface morphology. In the subsequent Li plating process, the morphology of Li deposition on the bare Li surface is slightly uneven after 15 min, along with some visible dendritic Li growth. With further increase of the Li plating time, continuous growth of mossy and dendritic Li can be observed on the surface of bare Li electrode. In comparison, the Bi-coated Li electrode guarantees uniform and smooth lithium deposition without dendritic Li growth even after 60 min. It can be concluded that the Li_xBi-rich layer is able to effectively suppress the formation of Li dendrite and stabilize the interface of Li metal anode. Fig. 4c and d illustrate the distinct Li electrodeposition behaviors on bare Li and Bi-coated Li electrodes. During the initial plating process, Li^+ deposits onto the anode surface and inevitably form rough and bump regions, causing the nonuniform distribution of local current density and Li ion flux on electrode surface. Moreover, the deposited Li reacts with organic electrolyte and eventually generates fragile and heterogeneous electrolyte-derived SEI. During further plating, Li dendrites would form and eventually puncture the electrolyte-derived SEI film, causing serious safety risks. While the MBE-deposited Bi film is alloyed to generate Li_xBi alloy phase at the beginning of Li plating, resulting in the following uniform deposition and dissolution of lithium throughout the Li_xBi-rich layer.

We also simulated the lithium deposition behaviors on bare Li and Bi-coated Li electrodes by using COMSOL Multiphysics [43,44]. The spatial

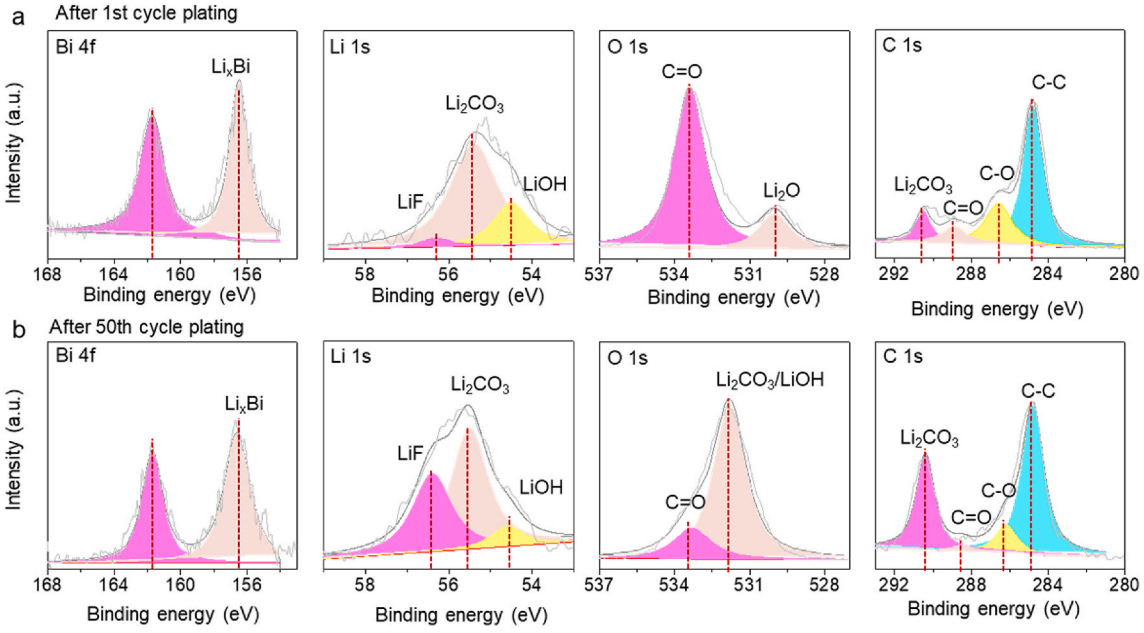

Fig. 3. XPS analysis of the SEI on cycled Bi-coated Li electrodes. (a, b) The Bi 4f, Li 1s, O 1s and C 1s XPS spectra of the Bi-coated Li electrodes after (a) the 1st and (b) the 50th cycles of Li plating, respectively.

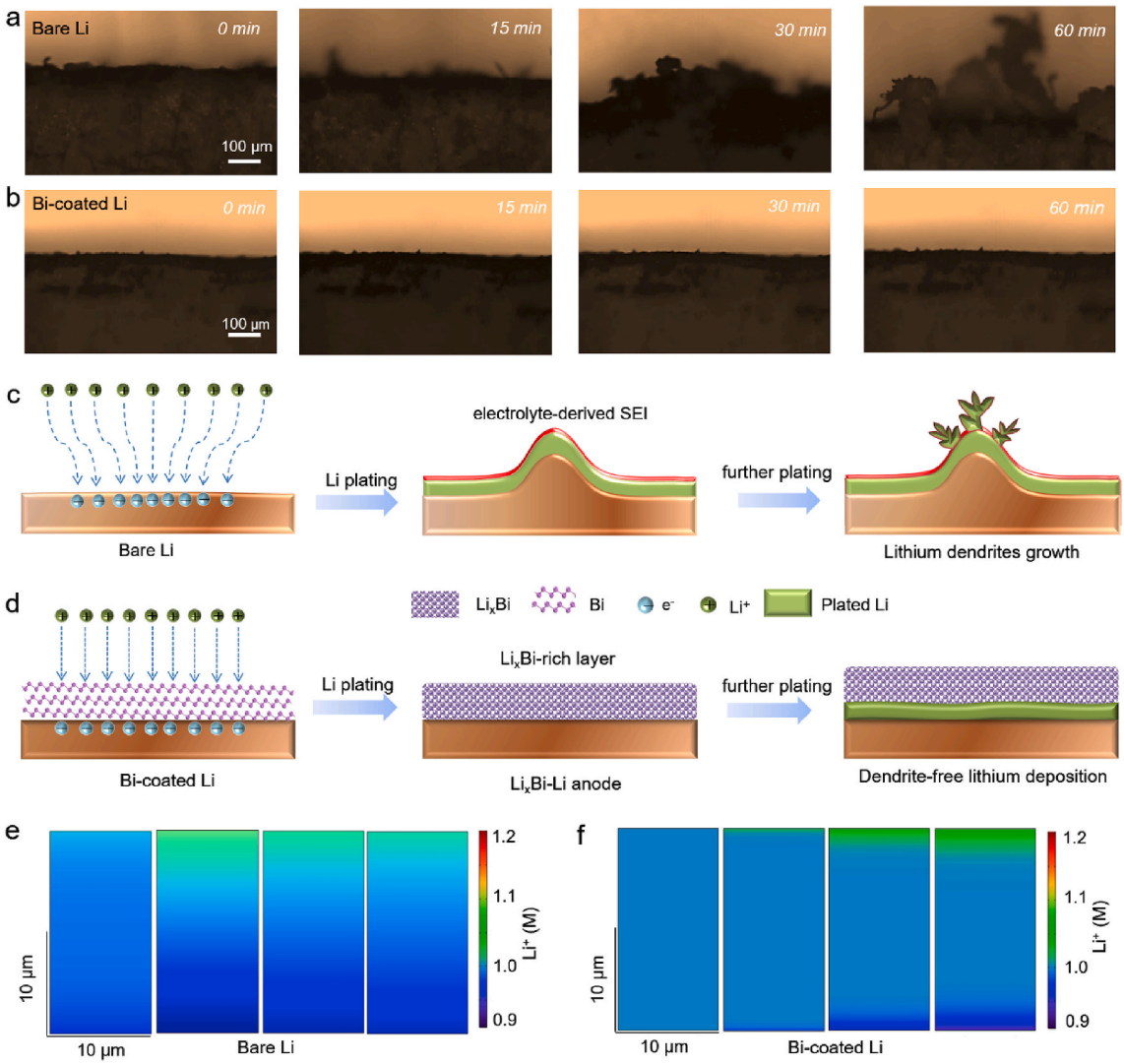

Fig. 4. Optical microscopy and protection mechanism of Bi-coated Li electrodes. (a, b) *Operando* optical microscopy observation of lithium electrodeposition on (a) bare Li and (b) Bi-coated Li electrodes at a current density of 3 mA cm^{-2}. (c, d) Schematic illustrations of the Li electrodeposition behavior on (c) bare Li and (d) Bi-coated Li electrodes. Due to the nonuniform distribution of electrical field on bare Li surface, Li tends to accumulate near protuberant regions, leading to the growth of Li dendrites. In contrary, the deposition and dissolution of lithium throughout the Li_xBi-rich layer on the Bi-coated Li electrode is quite uniform. (e, f) Computational simulation of the spatial distribution of Li ion flux on the SEI layers of (e) bare Li and (f) Bi-coated Li electrodes through COMSOL Multiphysics (from left to right: 1, 4, 10 s and equilibrium state).

distribution of Li ion flux on different SEI layers are modeled in Fig. S8 and Fig. 4e and f. Upon Li plating, routine SEI with poor ionic conductivity is formed on the surface of bare Li anode. It can be clearly seen that Li ions are incapable of distributing homogeneously near the routine SEI, resulting in uneven lithium deposition and dendrite formation. In contrast, a uniform distribution of Li ion flux could be achieved with the help of Li_xBi-rich layer on Bi-coated Li electrode, contributing to a dendrite-free Li electrodeposition behavior.

Atomic force microscopy (AFM) characterizations were employed to investigate the mechanical properties of the SEI formed on bare Li electrode and the Li_xBi-rich layer formed on Bi-coated Li electrode (Fig. 5a–h). As shown in Fig. 5a, the surface of SEI on bare Li electrode is very rough and exhibits numerous protuberances and holes, resulting from the growth of Li dendrites and corrosion of electrolyte. Notably, these granular protuberances will serve as the preferential sites for nonuniform deposition of Li near the electrode surface, eventually leading to the successive growth of dendritic or mossy Li structure. In contrast, the as-obtained Li_xBi-rich layer on Bi-coated Li electrode exhibits a relatively flat and smooth surface (Fig. 5e), which is helpful for achieving uniform Li nucleation and inhibiting Li dendrite growth, and also can prevent the parasitic reactions of underlying Li metal with the electrolyte. Fig. 5b, f displays the typical force-displacement curves of the routine SEI and Li_xBi-rich layer measured by AFM indentation. The routine SEI on bare Li electrode shows two parts of force curves (Fig. 5c), including an elastic-plastic deformation process in the surficial region and a plastic fracture process in the subjacent region [45]. For the Li_x-Bi-rich layer on Bi-coated Li electrode (Fig. 5g), a linear elastic region and fracture behavior can be found, suggesting that the Li_xBi-rich layer is very rigid and free of plasticity. The Young's moduli of the routine SEI and Li_xBi-rich layer were calculated based on the force-indentation curves. The average Young's modulus of the SEI on bare Li electrode is 3.4 ± 0.4 GPa (Fig. 5d). In contrast, the Li_xBi-rich layer on Bi-coated Li electrode has a much higher Young's modulus of 9.4 ± 0.3 GPa (Fig. 5h), which ensures Bi-coated Li electrode sufficient stiffness to suppress Li dendrite growth during the plating/stripping processes.

Coulombic efficiency is an important factor to evaluate the cycle life of Li metal-based batteries. For comparison, we deposited ultrathin Bi film with an ultrathin thickness of 40 nm on clean Cu foil (denoted as

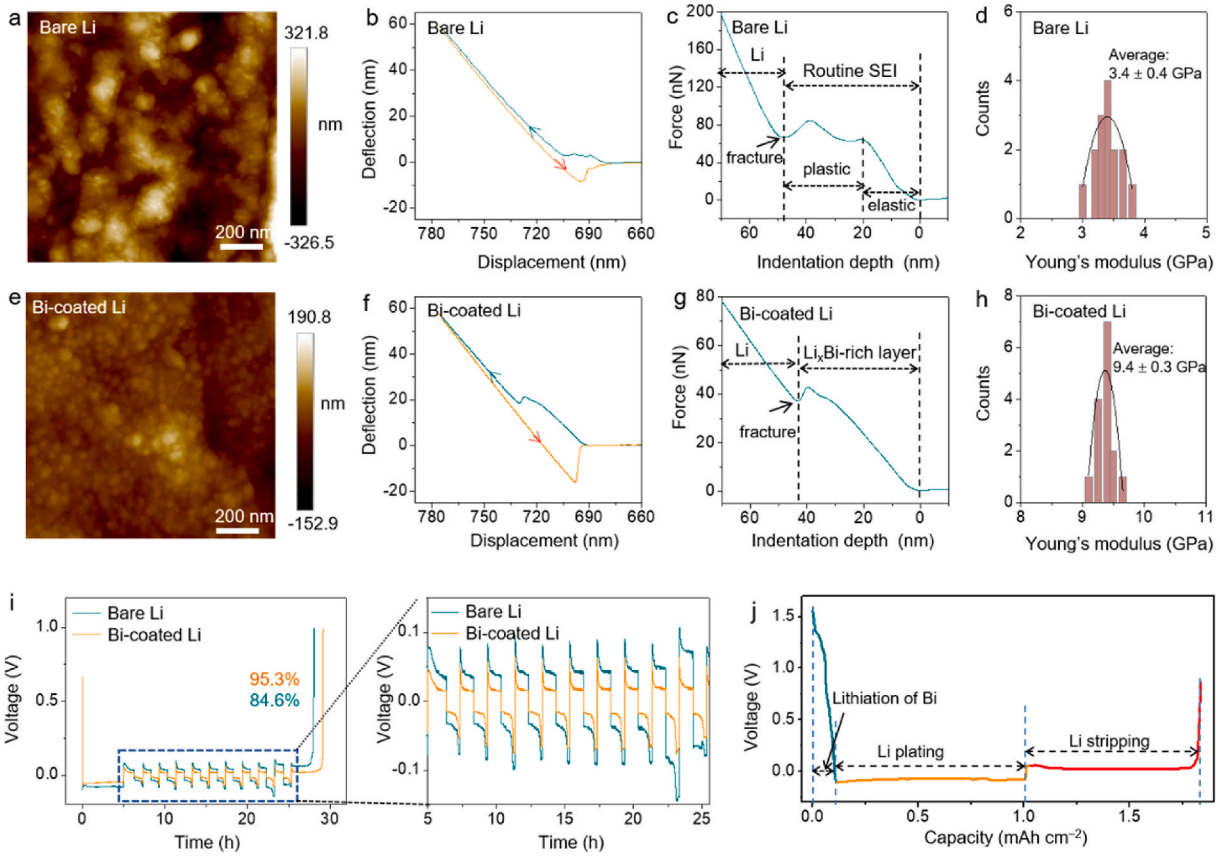

Fig. 5. AFM analysis of mechanical properties of the Li_xBi-rich layer layer. (a, e) AFM topography images, (b, f) typical force-displacement curves, (c, g) force-indentation curves of the routine SEI formed on bare Li electrode and the Li_xBi-rich layer formed on Bi-coated Li electrode, respectively. (d, h) The statistical histograms of Young's modulus calculated from the force-indentation curves of the routine SEI on bare Li electrode and the Li_xBi-rich layer on Bi-coated Li electrode, respectively. (i) Voltage-time curves for calculating the average Coulombic efficiencies of Li||Cu and Li||Bi–Cu asymmetrical cells cycled at 1 mA cm^{-2}. (j) Voltage profiles of Bi-coated Li electrode during (blue line) the initial lithiation process at a current density of 0.5 mA cm^{-2}, (yellow line) the subsequent Li plating process with an areal capacity of 1.0 mAh cm^{-2} at 0.5 mA cm^{-2}, and (red line) the stripping process at 0.5 mA cm^{-2}.

Bi–Cu) using the MBE apparatus, and then measured the Coulombic efficiencies of Li||Cu asymmetrical cells with bare Cu foil or Bi–Cu foil as working electrodes. The average Coulombic efficiencies were calculated based on a published method proposed by Aurbach et al. [46]. Firstly, the initial areal capacity of lithium deposited on bare Cu or Bi–Cu electrodes was set as 5.0 mAh cm^{-2} at a current density of 1 mA cm^{-2} (Fig. 5i). In the beginning, the ultrathin Bi film undergoes alloying reaction with Li to create a Li_xBi-rich layer. A limited capacity of 0.5 mAh cm^{-2} was stripped and plated at a current density of 0.5 mA cm^{-2} for 10 cycles. During these cycles, the average Coulombic efficiency of Bi–Cu electrode reaches 95.3%, while the bare Cu electrode only shows an average Coulombic efficiency of 84.6%. Notably, the lithiation process of Bi layer consumed the initial lithium deposition capacity. This is the main reason why the Coulombic efficiency is relatively low. The average Coulombic efficiency will be up to 98.8% if the lithiation capacity of Bi layer (0.21 mAh cm^{-2}) is removed from the initial deposited capacity of Li. The higher Coulombic efficiency of Bi–Cu electrode is mostly arisen from the protective Li_xBi-rich layer involved at the electrode/electrolyte interface, which effectively reduces electrolyte decomposition and irreversible consumption of active Li metal. Moreover, the interface polarization of Bi–Cu electrode is also lower than that of bare Cu electrode, indicating that the Li_xBi-rich layer can serve as lithiophilic interface to guide homogeneous nucleation and growth of Li metal. Fig. 5j displays the electrochemical Li plating/stripping process on the MBE-grown Bi film. An initial lithiation capacity of 0.21 mAh cm^{-2} was obtained by galvanostatic discharging the Li||Bi–Cu cell at a current density of 0.5 mA cm^{-2}. After the subsequent Li plating process up to a areal capacity of 1.0 mAh cm^{-2}, the cell can deliver a delithiation capacity of 0.78 mAh cm^{-2} at 0.8 V. This result suggests that the Li_xBi-rich layer can achieve highly reversible Li plating/stripping behavior.

To further investigate the composition distributions of the SEI formed on bare Li electrode and the Li_xBi-rich layer formed on Bi-coated Li electrode, XPS depth profiles were measured after 100 cycles at 2 mA cm^{-2} (Fig. S9). For cycled bare Li electrode, the Li 1s and C 1s XPS spectra imply that the routine SEI film is mainly composed of Li_2CO_3, LiOH, and LiF, originated from the decomposition products of electrolyte (Figs. S9a–c). After Ar-ion sputtering bombardment for different periods, Li_2CO_3 became the major component in the routine SEI layer on bare Li electrode. These XPS depth profiles illustrate that the routine SEI of bare Li electrode is too instable to protect underlying Li from the corrosion of electrolyte. In comparison, the Li_xBi-rich layer on Bi-coated Li electrode shows different composition distributions after cycling (Figs. S9d–f). The detail analysis of Li 1s, and C 1s XPS spectra confirm that Li_xBi alloy is the dominant component with a small fraction of Li_2CO_3 and LiF. After Ar-ion sputtering for different durations, the ratio of Li_2CO_3 gradually decreased, indicating its presence only on the upper surface of Li_xBi-rich SEI. This phenomenon also demonstrates that Li_xBi-rich layer can effectively reduce the formation of extra SEI and prevent the direct contact between lithium and electrolyte during cycling.

To demonstrate the feasibility of Bi-coated Li anode in workable batteries, both bare Li and Bi-coated Li anodes were paired with high-voltage $LiNi_{0.5}Co_{0.2}Mn_{0.3}O_2$ (NCM523) cathodes to assemble full cells. Fig. 6 displays the operation performances of Bi-coated Li||NCM523 and bare Li||NCM523 full cells. The initial discharge capacity of Bi-coated

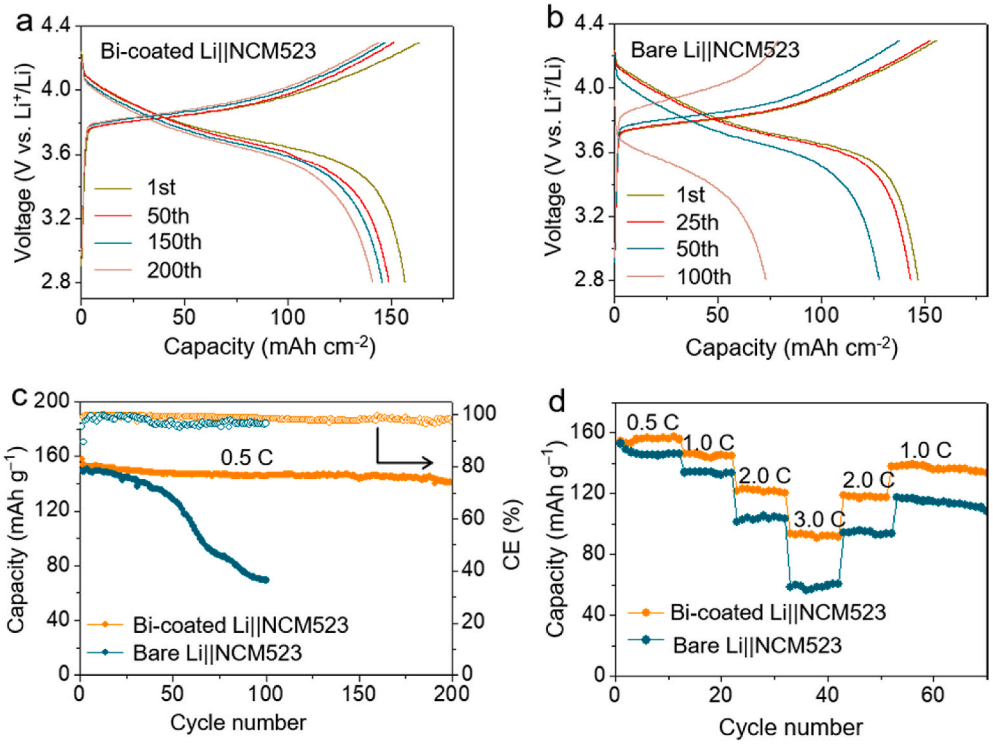

Fig. 6. Electrochemical performance of Bi-coated Li||NCM523 full cells. (a, b) Galvanostatic charge/discharge profiles of (a) Bi-coated Li||NCM523 and (b) bare Li||NCM523 full cells at 0.5C, respectively. (c) Cycling performances of Bi-coated Li||NCM523 and bare Li||NCM523 full cells at a current density of 0.5C (1 C = 180 mA g^{-1}). (d) Rate performances of Bi-coated Li||NCM523 and bare Li||NCM523 full cells at various current densities.

Li|NCM523 cell is 157.8 mAh g^{-1} at 0.5C, and an extraordinary capacity retention of 89.1% is still maintained after 200 cycles (Fig. 6a). In comparison, the bare Li||NCM523 full cell exhibits poor cycling performance with a low capacity retention of 47.2% after only 100 cycles at the same current density (Fig. 6b). Moreover, a stable Coulombic efficiency of more than 99.5% can be obtained by Bi-coated Li||NCM523 cell for 200 cycles, while the bare Li||NCM523 cell exhibits a slightly low Coulombic efficiency of ~98.1% after 100 cycles (Fig. 6c). These superior cycling performance and high Coulombic efficiency profit from highly stable and uniform Li_xBi-rich layer covered on Li metal surface, which can reinforce the ESI layer and inhibit the continuous consumption of fresh Li and electrolyte. Moreover, the Bi-coated Li||NCM523 cell also shows much better rate performance than the bare Li||NCM523 cell. Specifically, the Bi-coated Li||NCM523 cell delivered discharge capacities of 156, 146, 122, and 93 mAh g^{-1} corresponding to current densities of 0.5, 1.0, 2.0, and 3.0C, respectively; while the discharge capacity of bare Li||NCM523 cell is 155 mAh g^{-1} at 0.5C, and sharply falls to only ~50 mAh g^{-1} at the current density increased to 3.0C. The superior rate performance of Bi-coated Li||NCM523 cell demonstrates the realization of a smooth and uniform lithium deposition/dissolution behavior through ion-conducting Li_xBi-rich layer. To evaluate the stability of the MBE-grown Bi film, we also cycled Li metal batteries under lean electrolyte conditions. The amount of electrolyte used in the cell is 14 μL, corresponding to an electrolyte/cathode ratio of 4 μL mg^{-1}. As shown in Fig. S10, the Bi-coated Li||NCM523 cells had a capacity retention of 81.2% in 150 cycles under lean electrolyte condition. In contrast, the capacity of the bare Li||NCM523 control cell faded rapidly after 60 cycles. These results verify that the stable Li_xBi-rich alloy interface and reduced electrolyte loss decisively determine the cycling stability of Li metal batteries under lean electrolyte conditions.

3. Conclusions

In summary, a compact and ultrathin MBE-grown bismuth film on Li metal surface was proposed to guide uniform Li nucleation and achieve dendrite-free Li electrodeposition. Notably, the Bi-coated Li anode possesses outstanding moisture resistance in ambient air, benefiting from the high stability and compositional homogeneity of MBE-grown bismuth film. Upon Li plating, the electrochemically-active Bi film was transformed to lithiophilic Li_xBi alloy layer by in situ alloying reaction between lithium and bismuth. The as-formed Li_xBi-rich layer exhibits favorable charge transfer characteristics, mechanical properties and electrochemical stability. It can efficiently inhibit the parasitic side reactions between Li anode and electrolyte, and offer a smooth and homogeneous lithiophilic surface to regulate uniform lithium nucleation and growth. Moreover, the Li_xBi-rich layer can well maintain its structural integrity and multiple functions as a good protective barrier during long-term cycling in half and full cells. With these advantageous features, the Bi-coated Li anode exhibits excellent cycling stability for 300 h at 1 mA cm^{-2} with a small voltage polarization, and superior rate performance up to 5 mA cm^{-2}. The use of Li_xBi-rich alloy layer enables stable cycling of Li metal batteries under lean electrolyte. We hope this study may open a new avenue for the construction of artificial protective interphases for advanced Li-metal based rechargeable batteries.

Declaration of competing interest

The authors declare that they have no known competing financial interests or personal relationships that could have appeared to influence the work reported in this paper.

CRediT authorship contribution statement

Tao Chen: Writing - original draft. **Fanbo Meng:** Software. **Zewen Zhang:** Investigation. **Junchuan Liang:** Investigation. **Yi Hu:** Methodology. **Weihua Kong:** Investigation. **Xiao Li Zhang:** Resources. **Zhong Jin:** Conceptualization, Supervision, Writing - review & editing.

Acknowledgements

This work was supported by the National Key R&D Program (2017YFA0208200, 2016YFB0700600), the Fundamental Research Funds for the Central Universities (0205-14380219), the Projects of NSFC (21872069, 51761135104, 21573108), the Natural Science Foundation of Jiangsu Province (BK20180008, BK20170644), and the High-Level Innovation and Entrepreneurship Project of Jiangsu Province of China.

Appendix A. Supplementary data

Supplementary data to this article can be found online at https://doi.org/10.1016/j.nanoen.2020.105068.

References

[1] J.W. Choi, D. Aurbach, Nat. Rev. Mater. 1 (2016) 16013.
[2] D.C. Lin, Y.Y. Liu, Y. Cui, Nat. Nanotechnol. 12 (2017) 194–206.
[3] X.B. Cheng, R. Zhang, C.Z. Zhao, Q. Zhang, Chem. Rev. 117 (2017) 10403–10473.
[4] J.M. Tarascon, M. Armand, Nature 414 (2001) 359–367.
[5] L. Li, S. Basu, Y. Wang, Z. Chen, P. Hundekar, B. Wang, J. Shi, Y. Shi, S. Narayanan, N. Koratkar, Science 359 (2018) 1513–1516.
[6] L. Suo, Y.-S. Hu, H. Li, M. Armand, L. Chen, Nat. Commun. 4 (2013) 1481.
[7] A. Wang, S. Tang, D. Kong, S. Liu, K. Chiou, L. Zhi, J. Huang, Y.-Y. Xia, J. Luo, Adv. Mater. 30 (2018) 1703891.
[8] R. Cao, W. Xu, D. Lv, J. Xiao, J.-G. Zhang, Adv. Energy Mater. 5 (2015) 1402273.
[9] S. Jin, Z.W. Sun, Y. Guo, Z.K. Qi, C.K. Guo, X.H. Kong, Y.W. Zhu, H.X. Ji, Adv. Mater. 29 (2017) 1700783.
[10] H. Lee, S. Chen, X. Ren, A. Martines, V. Shutthanandan, M. Vijayakumar, K.S. Han, Q. Li, J. Liu, J.-G. Zhang, ChenSusChem 11 (2018) 3821–3828.
[11] W. Xu, J. Wang, F. Ding, X. Chen, E. Nasybutin, Y. Zhang, J.-G. Zhang, Energy Environ. Sci. 7 (2014) 513–537.
[12] M.D. Tikekar, S. Choudhury, Z. Tu, L.A. Archer, Nat. Energy 1 (2016) 16114.
[13] H. Zhang, G. Eshetu Gebrekidan, X. Judez, C. Li, M. Rodriguez-Martínez Lide, M. Armand, Angew. Chem. Int. Ed. 57 (2018) 2–28.
[14] Z.Q. Zeng, V.K. Murugesan, K.S. Han, X.Y. Jiang, Y.L. Cao, L.F. Xiao, X.P. Ai, H. X. Yang, J.-G. Zhang, M.L. Sushko, J. Liu, Nat. Energy 3 (2018) 674–681.
[15] W. Zhou, S. Wang, Y. Li, S. Xin, A. Manthiram, J.B. Goodenough, J. Am. Chem. Soc. 138 (2016) 9385–9388.
[16] X.G. Han, Y.H. Gong, K.K. Fu, X.F. He, G.T. Hitz, J.Q. Dai, A. Pearse, B.Y. Liu, H. Wang, G. Rubloff, Y.F. Mo, V. Thangadurai, E.D. Wachsman, L.B. Hu, Nat. Mater. 16 (2017) 572.
[17] A. Manthiram, X. Yu, S. Wang, Nat. Rev. Mater. 2 (2017) 16103.
[18] J.L. Hu, J. Tian, C.L. Li, ACS Appl. Mater. Interfaces 9 (2017) 11615–11625.
[19] L. Ma, C. Fu, L. Li, K.S. Mayilvahanan, T. Watkins, B.R. Perdue, K.R. Zavadil, B. A. Helms, Nano Lett. 19 (2019) 1387–1394.
[20] C.F. Li, S.H. Liu, C.G. Shi, G.H. Liang, Z.T. Lu, R.W. Fu, D.C. Wu, Nat. Commun. 10 (2019) 1363.
[21] H. Wu, Y. Cao, H. Su, C. Wang, Angew. Chem. Int. Ed. 57 (2018) 1361–1365.
[22] S. Choudhury, Z. Tu, S. Stalin, D. Vu, K. Fawole, D. Gunceler, R. Sundararaman, L. A. Archer, Angew. Chem. Int. Ed. 56 (2017) 13070–13077.
[23] G. Zheng, S.W. Lee, Z. Liang, H.W. Lee, K. Yan, H. Yao, H. Wang, W. Li, S. Chu, Y. Cui, Nat. Nanotechnol. 9 (2014) 618–623.
[24] X. Liang, Q. Pang, I.R. Kochetkov, M.S. Sempere, H. Huang, X.Q. Sun, L.F. Nazar, Nat. Energy 2 (2017) 17119.
[25] Z. Huang, G. Zhou, W. Lv, Y. Deng, Y. Zhang, C. Zhang, F. Kang, Q.-H. Yang, Nano Energy 61 (2019) 47–53.
[26] Q. Xu, J. Lin, C. Ye, X. Jin, D. Ye, Y. Lu, G. Zhou, Y. Qiu, W. Li, Adv. Energy Mater. 10 (2020) 1903292.
[27] J.-L. Ma, F.-L. Meng, Y. Yu, D.-P. Liu, J.-M. Yan, Y. Zhang, X.-B. Zhang, Q. Jiang, Nat. Chem. 11 (2019) 64–70.
[28] W. Li, H. Yao, K. Yan, G. Zheng, Z. Liang, Y.M. Chiang, Y. Cui, Nat. Commun. 6 (2015) 7436.
[29] F. Ding, W. Xu, G.L. Graff, J. Zhang, M.L. Sushko, X. Chen, Y. Shao, M. H. Engelhard, Z. Nie, J. Xiao, X. Liu, P.V. Sushko, J. Liu, J.G. Zhang, J. Am. Chem. Soc. 135 (2013) 4450–4456.
[30] N. Kamaya, K. Homma, Y. Yamakawa, M. Hirayama, R. Kanno, M. Yonemura, T. Kamiyama, Y. Kato, S. Hama, K. Kawamoto, A. Mitsui, Nat. Mater. 10 (2011) 682–686.
[31] R. Bouchet, S. Maria, R. Meziane, A. Aboulaich, L. Lienafa, J.-P. Bonnet, T.N. T. Phan, D. Bertin, D. Gigmes, D. Devaux, R. Denoyel, M. Armand, Nat. Mater. 12 (2013) 452–457.
[32] Y. Guo, H. Li, T. Zhai, Adv. Mater. 29 (2017) 1700007.
[33] W. Tang, X. Yin, S. Kang, Z. Chen, B. Tian, S.L. Teo, X. Wang, X. Chi, K.P. Loh, H.-W. Lee, G.W. Zheng, Adv. Mater. 30 (2018) 1801745.
[34] Y. Sun, Y. Zhao, J. Wang, J. Liang, C. Wang, Q. Sun, X. Lin, K.R. Adair, J. Luo, D. Wang, R. Li, M. Cai, T.K. Sham, X. Sun, Adv. Mater. 31 (2019) 1806541.
[35] R.A. Keegan, C. Zhao, M.N. Banis, Y. Zhao, R. Li, M. Cai, X. Sun, Angew. Chem. Int. Ed. 58 (2019) 15797–15802.
[36] Q. He, P. Li, Z. Wu, B. Yuan, Z. Luo, W. Yang, J. Liu, G. Cao, W. Zhang, Y. Shen, P. Zhang, S. Liu, G. Shao, Z. Yao, Adv. Mater. 31 (2019) 1901578.
[37] Y. Lu, W. Xu, M. Zeng, G. Yao, L. Shen, M. Yang, Z. Luo, F. Pan, K. Wu, T. Das, P. He, J. Jiang, J. Martin, Y.P. Feng, H. Lin, X.-S. Wang, Nano Lett. 15 (2015) 80–87.
[38] L. Kumari, J.H. Lin, Y.R. Ma, J. Phys. D Appl. Phys. 41 (2008), 025405.
[39] A. Reyes-Contreras, M. Camacho-Lopez, S. Camacho-Lopez, O. Olea-Mejia, A. Esparza-Garcia, J.G. Banuelos-Muneton, M.A. Camacho-Lopez, Opt. Mater. Express 7 (2017) 1777–1786.
[40] G.T. Zhou, O. Palchik, V.G. Pol, E. Sominski, Y. Koltypin, A. Gedanken, J. Mater. Chem. 13 (2003) 2607–2611.
[41] L. Suo, W. Xue, M. Gobet, S.G. Greenbaum, C. Wang, Y. Chen, W. Yang, Y. Li, J. Li, Proc. Natl. Acad. Sci. Unit. States Am. 115 (2018) 1156–1161.
[42] C. Yan, X.-B. Cheng, Y. Tian, X. Chen, X.-Q. Zhang, W.-J. Li, J.-Q. Huang, Q. Zhang, Adv. Mater. 30 (2018) 1707629.
[43] H. Chen, A. Pei, D. Lin, J. Xie, A. Yang, J. Xu, K. Lin, J. Wang, H. Wang, F. Shi, D. Boyle, Y. Cui, Adv. Energy Mater. 9 (2019) 1900858.
[44] J.-Y. Liang, X.-X. Zeng, X.-D. Zhang, T.-T. Zuo, M. Yan, Y.-X. Yin, J.-L. Shi, X.-W. Wu, Y.-G. Guo, L.-J. Wan, J. Am. Chem. Soc. 141 (2019) 9165–9169.
[45] J. Huang, X. Guo, X. Du, X. Lin, J.-Q. Huang, H. Tan, Y. Zhu, B. Zhang, Energy Environ. Sci. 12 (2019) 1550–1557.
[46] D. Aurbach, Y. Gofer, J.J. Langzam, J. Electrochem. Soc. 136 (1989) 3198–3205.

Tao Chen received his Ph.D. degree in Chemical Engineering and Technology at Nanjing University of Science and Technology in June 2015. He worked as a postdoctoral scholar at Nanjing University in the group of Prof. Zhong Jin (2015–2019). He is currently a research fellow at National University of Singapore. His current research focuses on the design and synthesis of nanostructured electrode materials for rechargeable batteries.

Fanbo Meng received his Bachelor's degree in Packaging Engineering from Kunming University of Science and Technology in 2016. He is now pursuing his Ph.D degree under the supervision of Prof. Jin Huang in School of Mechatronic Engineering at Xidian University. His research interests include computational fluid dynamics and 3D printing sintering process.

Zewen Zhang received his Bachelor's degree from School of Chemistry and Chemical Engineering, Nanjing University in 2018. He is currently pursuing his master degree under the supervision of Prof. Zhong Jin at the same school. His research interests focus on improving properties of lithium metal batteries.

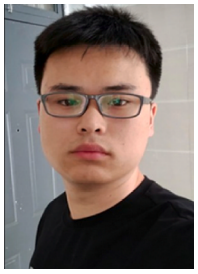

Junchuan Liang received his B.S. degree from the College of Chemistry and Chemical Engineering of Lanzhou University in 2019. Now he is pursuing his Ph.D. degree under the supervision of Prof. Zhong Jin at School of Chemistry and Chemical Engineering at Nanjing University. His research interest focuses on the application of the 2D nano-materials grown through the MBE.

Yi Hu received his B.S. degree in Chemistry from Sichuan University in 2014. He has obtained his Ph.D. degree in 2019 under the supervision of Prof. Zhong Jin in School of Chemistry and Chemical Engineering at Nanjing University. His research interests reside in two-dimensional nanomaterials for electrochemical energy storage and photoelectric conversion.

Weihua Kong received his B.S. degree in Chemistry from Hunan University in 2017. He is now pursuing his M.S degree under the supervision of Prof. Zhong Jin in School of Chemistry and Chemical Engineering at Nanjing University. His research interest is mainly concentrated on the lithium-sulfur and lithium-metal batteries.

Xiao Li Zhang received her Ph.D. degree from Zhengzhou University in 2011, and worked as a visiting scholar at University of Toronto (2012–2013). Now she is an associate professor in School of Materials Science and Engineering at Zhengzhou University.

Zhong Jin received his B.S. (2003) and Ph.D. (2008) in chemistry from Peking University. He worked as a postdoctoral scholar at Rice University (2008–2010) and Massachusetts Institute of Technology (2010–2014). Now he is a professor in School of Chemistry and Chemical Engineering at Nanjing University. He leads a research group working on advanced materials and devices for energy conversion and storage.